Gear Collision Reduction of In-wheel-motor by Joint Torque Control Using Load-side High-resolution Encoder

Seigo Wakui, Tomoki Enmei, Hiroshi Fujimoto, Yoichi Hori
The University of Tokyo
5-1-5, Kashiwanoha, Kashiwa, Chiba, 277-8561, Japan
Email : wakui.seigo18@ae.k.u-tokyo.ac.jp

Kenji Omata
Nikon Corporation Sendai Branch
277, Tako Aza-hara, Natori, Miyagi, 981-1221, Japan
Email : Kenji.Omata@nikon.com

***Abstract*—In-wheel-motors (IWMs) are attracting considerable attentions as drivetrain for electric vehicles (EVs) owing to their high motion performance. Requirement of large motor torque with limited mounting space for IWMs expects a geared drivetrain, but the geared structure deteriorates control performance and ride comfort by collisions of gear teeth. In order to reduce the vibration by collisions, a joint torque control for the two-inertia system using load-side encoders is applied to reduction geared IWMs (RG-IWMs). This paper focuses on vehicle starting phase when gear collisions appear seriously. Simulations and experiments demonstrate that joint torque of RG-IWMs can be precisely controlled and the vibration by collisions can be sufficiently suppressed.**

***Index Terms*—In-wheel-motor, two-inertia system, backlash compensation, joint torque control, load-side encoder.**

I. Introduction

Electric vehicles (EVs) are gathering considerable attentions due to a greater deal of the concern for environmental problems [1], and a lot of studies on EVs have been done [2], [3]. Advantages of EVs are not only their environmental benefits but also their high motion performance.

EVs can be classified into on-board motor EVs and in-wheel-motor EVs (IWM-EVs) according to the arrangement of motors. The performance of on-board motor EVs is limited by low frequent resonance of long drive shafts, while that of IWM-EVs can be enhanced thanks to short shafts [4] as indicated in the successful studies on various traction control methods [5], [6]. Since the required specifications for IWMs are severe (e.g. large maximum torque, limited mounting space, and cost etc.), reduction geared IWMs (RG-IWMs) are feasible to address these requirements [7].

It is difficult to control a system with gears due to backlash, which is a mechanical gap between gear teeth. The vibration caused by gear collisions due to backlash has been regarded as a serious problem and has been studied for effective compensation for decades [8]–[10]. However, most of the studies assume the industrial robot appilications, and the number of studies which propose vibration suppresion methods for EVs is limited [11]. Therefore, the effective backlash compensation method for EVs remains to be proposed.

In this paper, we propose a novel application of joint torque control to RG-IWMs. Joint torque control makes it possible to control gear torque precisely, which enables gear collision reduction and vibration suppression. Various joint torque control methods are applied mainly in the industrial robotic field and require different sensor configurations (e.g. only motor-side encoders in [12], joint torque sensors in [13], [14], both motor-side and load-side encoders in [15], [16]). In these studies, a system with gears is modeled as the two-inertia system, where a motor and a load are connected with rigid gears. With only motor-side encoders, it is difficult to compensate backlash and suppress the vibration due to the unknown load-side position, while with joint torque sensors or both motor-side and load-side encoders, the effective backlash compensation and vibration suppression can be realized. However, mounting joint torque sensors on EVs is not practical in point of cost. Therefore, our research group has proposed a novel RG-IWMs structure with both motor-side and load-side encoders for advanced EVs motion control. Joint torque control using load-side information can be applied to our developed vehicle.

This paper focuses on the vehicle starting phase, when gear collisions appear severely. The number and impact of collisions are reduced by effective application of the joint torque control proposed in our previous study [17]. The joint torque control method uses both motor-side and load-side encoders and considers the dynamics of the two-inertia system and the backlash nonlinearity. This proposed method enables the motor side to mesh with the load side even under disturbance from a road. The effectiveness of the proposed method is validated through simulations and experiments, compared to that of the conventional method which does not consider the dynamics of the two-inertia system and the backlash nonlinearity.

II. Experimental Setup

A. Experimental Vehicle

The experimental vehicle shown in Fig. 1 is used as an experimental vehicle. Our research group developed it based on the commercial EV "i-MiEV" produced by Mitsubishi Motors Corporation. The two rear motors of the experimental vehicle are RG-IWMs with both motor-side and load-side encoders.

Fig. 1. Experimental vehicle "FPEV4-Sawyer".

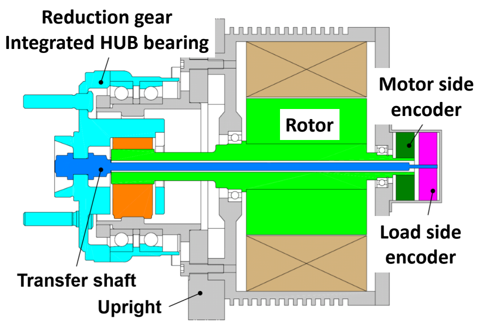

Fig. 2. Developed RG-IWM unit with a load-side encoder.

The details of developed RG-IWMs unit are described in the next subsection.

B. RG-IWM Unit with Load-side High-resolution Encoder

Fig. 2 shows a schematic of our developed RG-IWM unit. It has both motor-side and load-side encoders, which are manufactured by Nikon corporation, and their resolution is 20 bit. Because of backlash, gear torsion and road disturbance, it is difficult to obtain the angle of the load precisely using only motor-side encoders, while load-side encoders make it possible to measure the precise angle of the load side. The load-side encoder and the load side are connected with a transfer shaft. Mechanical resonance frequency of the transfer shaft is sufficiently high because the shaft rigidity is high and the inertia of a load-side encoder is very small. Therefore, the shaft does not affect the controllability of RG-IWM and the unit can be modeled as the two-inertia system as described in the next subsection.

C. RG-IWM Unit Model

The developed IWM unit can be modeled as the two-inertia system to consider its gear torsion and backlash. The equations of rotational motion are expressed as (1)-(5) :

TABLE I
DEFINITION OF PLANT PARAMETERS

Plant parameters	Definition
Motor inertia	J_m
Load inertia	J_l
Motor angular velocity	ω_m
Load angular velocity	ω_l
Joint torsional angular velocity	$\Delta\omega$
Motor angle	θ_m
Load angle	θ_l
Joint torsional angle	$\Delta\theta$
Motor torque	T_m
Joint torque	T_s
Joint elasticity	K
Backlash width	L
Gear ratio	g
Half of vehicle mass	M
Half of vehicle normal force	N
Vehicle speed	V
Wheel speed	V_ω
Driving force	F_d
Driving resistance	F_r
Tire radius	r

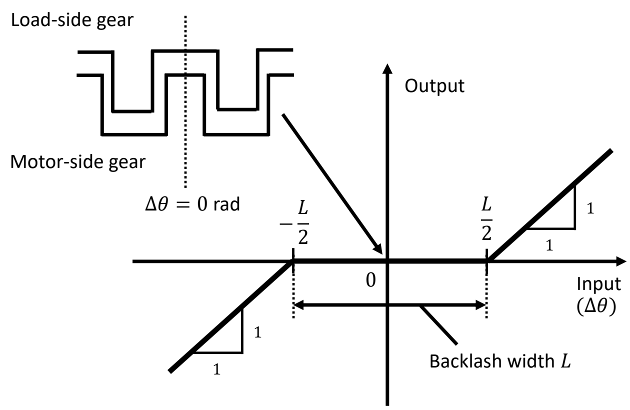

Fig. 3. Deadzone function $\mathrm{bl}(\Delta\theta)$.

$$J_m\dot{\omega}_m = T_m - T_s, \tag{1}$$
$$J_l\dot{\omega}_l = gT_s - rF_d, \tag{2}$$
$$T_s = K \cdot \mathrm{bl}(\Delta\theta) \tag{3}$$
$$= K \cdot \mathrm{bl}\left(\frac{\Delta\omega}{s}\right) \tag{4}$$
$$= K \cdot \mathrm{bl}\left(\frac{\omega_m - g\omega_l}{s}\right). \tag{5}$$

The definition of parameters is shown in TABLE I. Backlash is modeled by deadzone function $\mathrm{bl}(\Delta\theta)$ expressed as (6) and shown in Fig. 3.

$$\mathrm{bl}(\Delta\theta) = \begin{cases} \Delta\theta + \frac{L}{2} & \left(\Delta\theta < -\frac{L}{2}\right), \\ 0 & \left(-\frac{L}{2} \leq \Delta\theta \leq \frac{L}{2}\right), \\ \Delta\theta - \frac{L}{2} & \left(\Delta\theta > \frac{L}{2}\right). \end{cases} \tag{6}$$

The origin in Fig. 3 is defined as the position where the motor side and the load side are located in the middle of backlash. From (1)-(5), the block diagram of a RG-IWM unit model

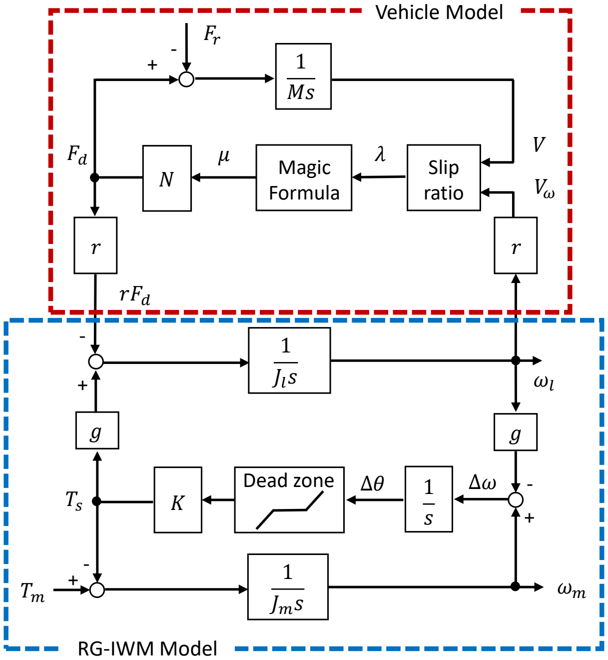

Fig. 4. Block diagram of a RG-IWM and a vehicle model.

is expressed as the area surrounded by blue dotted line in Fig. 4. In this paper, two RG-IWM units equipped in rear left and right wheels are assumed to have the same physical characteristics.

D. Vehicle Model

In this paper, only longitudinal motion of a vehicle is considered, and steering and lateral motion are not taken into consideration. The equation of longitudinal motion is expressed as (7) :

$$M\dot{V} = F_d - F_r. \tag{7}$$

The definition of parameters is shown in TABLE I. F_r is neglected since it is much smaller than F_d when the vehicle starts. Our vehicle is driven by two rear IWMs. Therefore, half-car model is adopted in this paper. M and N equals half of the whole vehicle mass and half of the whole vehicle normal force respectively. Driving force is generated by a slip, which is physical quantity indicating an amount of a wheel slip. Slip ratio λ is defined as (8) :

$$\lambda = \frac{r\omega_l - V}{\max(r\omega_l,\, V,\, \epsilon)}. \tag{8}$$

ϵ is the minute value to avoid zero denominator. Relationship between λ and friction coefficient μ is expressed by magic formula shown in (9), which is one of famous models for this relation [18] :

$$\mu(\lambda) = D\sin\left(C\tan^{-1}B\left((1-E)\,\lambda + \frac{E}{B}\tan^{-1}(B\lambda)\right)\right). \tag{9}$$

From (7)-(9), the block diagram of a vehicle model is expressed as the area surrounded by red dotted line in Fig. 4.

TABLE II
SYMBOLS IN THE BLOCK DIAGRAM OF THE JOINT TORQUE CONTROL

Controller parameters	Definition
P controller of motor angular velocity	C_p
PI controller of joint torque	C_{PI}
Nominal motor inertia	J_{mn}
Joint torque reference	T_s^*
Estimated joint torque	$\hat{T}_s$
Nominal torsional elasticity	K_n
Joint torsional angular velocity reference	$\Delta\omega^*$
LPF of joint torque estimator	$Q_{TsOB}(s)$
First order LPF of reaction force observer RFOB	$Q_{RFOB}(s)$
First order LPF to realize motor angular velocity FF control	$Q_{\omega_m FF}(s)$
First order LPF to realize joint torque FF control	$Q_{TsFF}(s)$

Here, notice that the vehicle model is used only for calculating the driving force accurately in simulations, not for designing controllers.

III. Joint Torque Control Using Load-side High-resolution Encoder

The block diagram of the proposed joint torque control for collision reduction is shown in Fig. 5. It is based on [17] proposed by our research group. The symbols in the block diagram of the joint torque control are shown in TABLE II. Suffix n denotes nominal values and superscript $*$ means reference values.

In the proposed method, torsional angular velocity is controlled using a feedforward (FF) and a feedback controller to control joint torque.

First, the joint torque feedforward controller is designed based on an inverse model of the plant as follows. The feedforward controller compensates for backlash and improves the performance of reference tracking. It makes possible to control joint torque precisely. The reference of joint torsional angular velocity is generated from the reference of joint torque. From Fig. 5, the relationship between $\Delta\omega$ and T_s is obtained as (10) :

$$T_s = K \cdot \mathrm{bl}\left(\frac{1}{s}\Delta\omega\right). \tag{10}$$

Then, following (11) can be obtained :

$$\Delta\omega^* = \mathrm{bl}^{-1}\left(\frac{T_s{}^*}{K}\right)\cdot s \cdot Q_{T_sFF}(s). \tag{11}$$

The first order low pass filter (LPF) Q_{TsFF} is applied to make the transfer function proper. Here, the inverse function of deadzone is not differentiable. Therefore, using the sigmoid function, expressed as (12) and shown in Fig. 6, the novel differentiable inverse deadzone model expressed as (13) is used as the approximate inverse model of deadzone :

$$\zeta(x) = K_{sig}\left(\frac{1}{1+e^{-ax}} - \frac{1}{2}\right), \tag{12}$$

$$\zeta_p(x) = \begin{cases} x + x_1 + \zeta(-x_1) & (x < -x_1), \\ \zeta(x) & (-x_1 \le x \le x_1), \\ x - x_1 + \zeta(x_1) & (x > x_1). \end{cases} \tag{13}$$

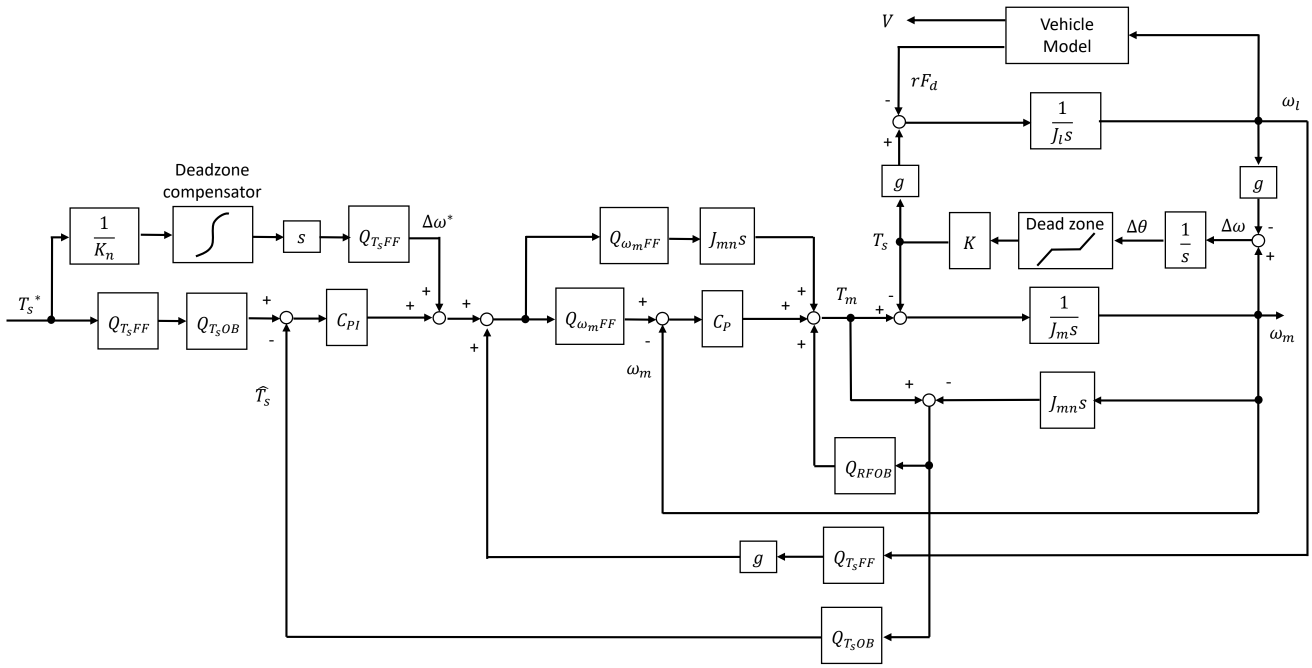

Fig. 5. Block diagram of the proposed joint torque control using load-side high-resolution encoder [17].

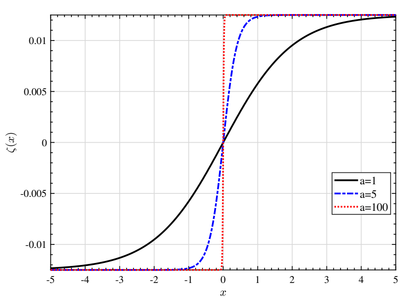

Fig. 6. Sigmoid function ($K_{sig} = 0.025$).

K_{sig} means the total gain and a is the gain determining the similarity to the inverse function of deadzone model and they are tuning parameters. x_1 is located on the point where the slope of sigmoid function is 1.

Secondary, the joint torque feedback controller is designed as follows. The joint torque is estimated by reaction force observer (RFOB) and controlled with PI controller. The first order LPF Q_{TsOB} is applied to make the inverse plant proper. The PI controller is designed by the pole placement to the plant, $T_s = K\frac{1}{s}\Delta\omega$. Here, the delay of Q_{TsOB} has to be considered. Therefore, Q_{TsOB} is also applied to the reference value generation of the joint torque. The reference of ω_m is generated using the reference of $\Delta\omega$.

Finally, ω_m is controlled in the minor loop with feedforward and P feedback controller. By using feedforward controller, high control bandwidth is achieved. High bandwidth is required to compensate backlash quickly and it improves the performance of the outer loop. From Fig. 5, the torsional angular velocity $\Delta\omega$ is obtained as (14) :

$$\Delta\omega = \omega_m - g\omega_l. \tag{14}$$

Then, following (15) can be obtained :

$$\omega_m{}^* = \Delta\omega^* + g\omega_l. \tag{15}$$

From (15), the reference of ω_m is generated from the reference of $\Delta\omega$ using ω_l, which can be obtained with load-side encoders.

IV. Simulations

A. Conventional Method

To evaluate the effectiveness of the proposed method, a conventional method is introduced. In the conventional method, the reference of the motor torque is set and the motor torque is controlled. Notice that this method does not consider the dynamics of the two-inertia system and backlash nonlinearity.

B. Simulation Conditions

The parameters used in the simulations are shown in TABLE III. The P controller of motor angular velocity and the cutoff frequency of RFOB are designed such that the inner bandwidth become as high as possible considering the stable margin. The PI controller is designed based on pole placement such that the poles are placed at 5 Hz. $\epsilon = 1e{-}5$ is introduced in (8) to avoid zero denominator and $B = 11.43$, $C = 1.314$, $D = 1$, $E = -0.225$ is adopted in (9), which determine the slip ratio and the relationship between λ and μ. The joint torque reference in the proposed method is set to be ramp function which increases to 64 Nm in 10 s and the saturation is set to be 64 Nm. This reference supposes gradual acceleration. The motor torque

TABLE III
SIMULATION PARAMETERS

Parameters	Value
Half of vehicle Mass M	$650\,\mathrm{kg}$
Half of vehicle normal force N	$6370\,\mathrm{N}$
Tire radius r	$0.3\,\mathrm{m}$
Motor inertia J_m	$0.3\,\mathrm{kgm/s^2}$
Nominal motor inertia J_{mn}	$0.3\,\mathrm{kgm^2}$
Load inertia J_l	$1.13\,\mathrm{kgm/s^2}$
Joint elasticity K	$600\,\mathrm{Nm/rad}$
Nominal joint elasticity K_n	$600\,\mathrm{Nm/rad}$
Gear ratio g	4.1739
Backlash width L	$0.0366\,\mathrm{rad}$
Gain of P controller	10
Pole of PI controller	$5\,\mathrm{Hz}$
Cutoff frequency of Q_{TsOB}	$50\,\mathrm{Hz}$
Cutoff frequency of Q_{RFOB}	$50\,\mathrm{Hz}$
Cutoff frequency of $Q_{\omega_m OB}$	$50\,\mathrm{Hz}$
Cutoff frequency of Q_{TsFF}	$50\,\mathrm{Hz}$
Total gain of sigmoid function K_{sig}	0.025
Similarity gain a	10000

reference of the conventional method is determined to make the vehicle speed equal that of the proposed method for fair comparison. The motor torque reference of the conventional method is ramp function which increases to $70\,\mathrm{Nm}$ in $10\,\mathrm{s}$ and the saturation is set to be $70\,\mathrm{Nm}$. This conventional method also supposes gradual acceleration. The initial position of gears is determined to make joint torsional angle equal minus half of backlash width, when gear collisions appear most severely.

C. Simulation Results

Fig. 7(a) shows the vehicle speed of the proposed and conventional methods. They are almost same and the fair comparison is realized. Fig. 7(b) shows the motor torque of the proposed and conventional methods. The motor torque of the conventional method is controlled to follow the reference, while the motor torque of the proposed method vibrates to make joint torque follow the reference around gear collisions. Fig. 7(c) shows the joint torque of the proposed and conventional methods. The joint torque of the proposed method follows the reference and the estimated joint torque follows the joint torque of the proposed method accurately, while the joint torque of the conventional method vibrates after gear collisions. Fig. 7(d) shows the joint torsional angle. Here, the black dotted lines mean the border of backlash. The number and impact of gear collisions of the proposed and conventional methods are compared. The number of gear collisions of the proposed method is one and two smaller than that of the conventional method. In addition to it, the maximum joint torque, which expresses the impact of gear collision, is $9.5\,\mathrm{Nm}$ in the proposed method, while $4.3\,\mathrm{Nm}$ in the conventional method, that is, the impact is decreased by $54.7\,\%$. These results show the effectiveness of applying the joint torque control to gear collision reduction of RG-IWMs.

V. EXPERIMENTS

A. Experimental Conditions

The nominal motor inertia J_{mn}, the nominal torsional elasticity K_n, and P and PI controller gains used in the experiments are same as those in the simulations. The cutoff frequency of LPF, the total gain of sigmoid function K_{sig} and the similarity gain a are experimentally tuned. In the beginning, minute minus motor torque is inputted and the motor side and load side are meshed with each other. After that, the conventional and proposed methods are implemented and the experimental vehicle starts acceleration on a flat asphalt road shown in Fig. 1.

B. Experimental Results

Fig. 8(a) shows the motor torque of the proposed and conventional methods. This experimental comparison corresponds to Fig. 7(b) . Fig. 8(b) shows the reference of the joint torque and the estimated joint torque of the proposed method. The estimated joint torque of the proposed method follows the reference. However, the noise of the motor speed or modeling error generates an error. In estimating the joint torque, the motor angular velocity obtained by differentiating the motor angle is used. Therefore, the noise in the motor angle makes the estimated joint torque vibrate. Fig. 8(c) shows the joint torsional angle of the proposed joint torque control and the conventional motor torque control. Here, the black dotted lines mean the border of backlash. The number of gear collisions of the proposed method is reduced compared to that of the conventional method. Therefore, the effectiveness of the proposed method is validated through the experiments. The results of the experiments correspond to those of the simulations. Therefore, modeling RG-IWMs as the two-inertia system is proper.

VI. CONCLUSION

IWMs are attracting considerable attentions owing to their high motion performance. Requirement of large motor torque with limited mounting space for IWMs expects a geared drive-train, but the geared structure deteriorates control performance and ride comfort by collisions of gear teeth. In this paper, joint torque control for the two-inertia system is applied to RG-IWMs to reduce gear collisions when RG-IWMs start. Simulations and experiments reveal the effectiveness of the proposed method. The number of collisions and the maximum joint torque, which expresses the impact of gear collisions, are reduced in the proposed method compared to the conventional method. This paper contributes to overcoming the weakness of RG-IWMs by precise joint torque control with backlash compensation. Gear collisions only when starting are considered in this paper. In future works, gear collision reduction in other situations has to be considered.

ACKNOWLEDGMENT

This work was partly supported by JSPS KAKENHI Grant Number 18H03768. Finally, the authors would like to express their deepest appreciation to Toyo Denki Seizo K.K and NSK

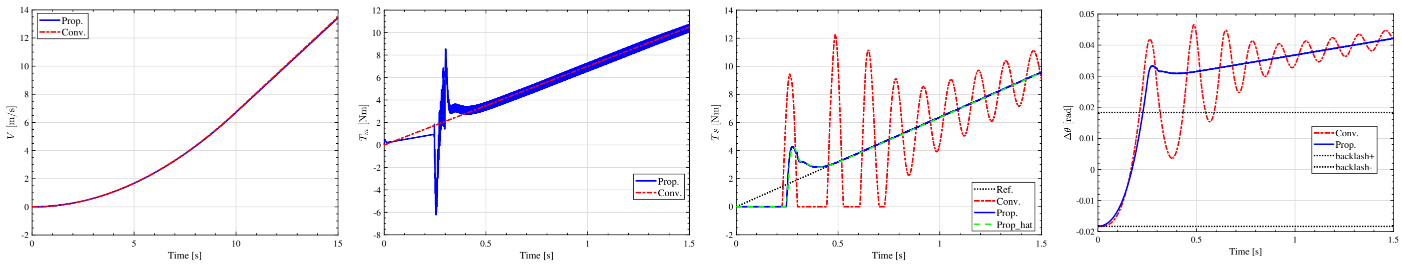

(a) Vehicle speed V.

(b) Motor torque T_m.

(c) Joint torque T_s.

(d) Joint torsional angle $\Delta\theta$.

Fig. 7. Simulation results.

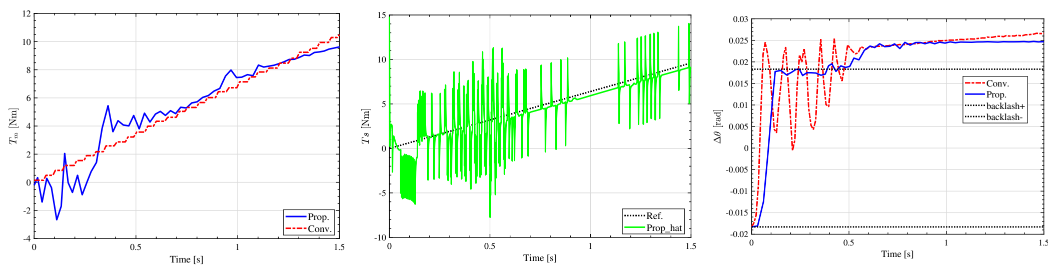

(a) Motor torque T_m.

(b) Estimated joint torque $\hat{T}_s$.

(c) Joint torsional angle $\Delta\theta$

Fig. 8. Experimental results.

for providing the inverter, the motor, and the gear used in the experiments.

References

[1] Y. Hori, “Future vehicle driven by electricity and control - Research on four-wheel-motored ”UOT Electric March II”,” *IEEE Transactions on Industrial Electronics*, vol. 51, no. 5, pp. 954–962, 2004.

[2] V.-D. Doan, H. Fujimoto, T. Koseki, T. Yasuda, H. Kishi, and T. Fujita, “Simultaneous Optimization of Speed Profile and Allocation of Wireless Power Transfer System for Autonomous Driving Electric Vehicles,” *IEEJ Journal of Industry Applications*, vol. 7, no. 2, pp. 189–201, 2018.

[3] K. Itoh, S. Inoue, M. Ishigaki, T. Sugiyama, and T. Umeno, “Power loss estimation for three-port DC/DC converter for 12-V/48-V dual-voltage hybrid electric vehicle subsystem,” *IEEJ Transactions on Electrical and Electronic Engineering*, vol. 13, no. 7, pp. 1060–1070, 2018.

[4] S. Murata, “Innovation by in-wheel-motor drive unit,” *Vehicle System Dynamics*, vol. 50, no. 6, pp. 807–830, 2012.

[5] M. Yoshimura and H. Fujimoto, “Driving Torque Control Method for Electric Vehicle with In-Wheel Motors,” *IEEJ Transactions on Industry Applications*, vol. 131, no. 5, pp. 721–728, 2011.

[6] W.-P. Chiang, D. Yin, M. Omae, and H. Shimizu, “Integrated Slip-Based Torque Control of Antilock Braking System for In-Wheel Motor Electric Vehicle,” *IEEJ Journal of Industry Applications*, vol. 3, no. 4, pp. 318–327, 2014.

[7] T. Makino, “Recent technology trend of in-wheel motor system for automotive vehicle,” *Toraibarojisuto/Journal of Japanese Society of Tribologists*, vol. 58, no. 5, pp. 310–316, 2013.

[8] K. Yuki, T. Murakami, and K. Ohnishi, “Vibration control of 2 mass resonant system by resonance ratio control,” *Proceedings of IECON ’93 - 19th Annual Conference of IEEE Industrial Electronics*, pp. 2009–2014, 1993.

[9] M. Nordin and P. O. Gutman, “Controlling mechanical systems with backlash - A survey,” *Automatica*, vol. 38, no. 10, pp. 1633–1649, 2002.

[10] D. K. Prasanga, E. Sariyildiz, and K. Ohnishi, “Compensation of Backlash for Geared Drive Systems and Thrust Wires Used in Teleoperation,” *IEEJ Journal of Industry Applications*, vol. 4, no. 5, pp. 514–525, 2015.

[11] J. Motosugi, O. Sho, S. Akira, and F. Kengo, “Motor Control Technologies for Improving the Driving Performance of Electric Vehicles,” *EVS31&EVTeC*, 2018.

[12] M. Ruderman and M. Iwasaki, “Sensorless Torsion Control of Elastic-Joint Robots with Hysteresis and Friction,” *IEEE Transactions on Industrial Electronics*, vol. 63, no. 3, pp. 1889–1899, 2016.

[13] T. Kawakami, K. Ayusawa, H. Kaminaga, and Y. Nakamura, “High-fidelity joint drive system by torque feedback control using high precision linear encoder,” *Proceedings - IEEE International Conference on Robotics and Automation*, pp. 3904–3909, 2010.

[14] P. Weiss, P. Zenker, and E. Maehle, “Feed-forward friction and inertia compensation for improving backdrivability of motors,” *2012 12th International Conference on Control, Automation, Robotics and Vision, ICARCV 2012*, pp. 288–293, 2012.

[15] C. Mitsantisuk, M. Nandayapa, K. Ohishi, and S. Katsura, “Design for Sensorless Force Control of Flexible Robot by Using Resonance Ratio Control Based on Coefficient Diagram Method,” *Automatika Journal for Control, Measurement, Electronics, Computing and Communications*, vol. 54, no. 1, 2013.

[16] S. Oh and K. Kong, “High-Precision Robust Force Control of a Series Elastic Actuator,” *IEEE/ASME Transactions on Mechatronics*, vol. 22, no. 1, pp. 71–80, 2017.

[17] S. Yamada, K. Inukai, H. Fujimoto, K. Omata, Y. Takeda, and S. Makinouchi, “Joint torque control for two-inertia system with encoders on drive and load sides,” *Proceeding - 2015 IEEE International Conference on Industrial Informatics, INDIN 2015*, vol. 1, pp. 396–401, 2015.

[18] H. B. Pacejka and E. Bakker, “The Magic Formula Tyre Model,” *Vehicle System Dynamics : International Journal of Vehicle Mechanics and Mobility*, vol. 21, no. 1, pp. 1–18, 1922.